Intracellular Uptake and Trafficking of Difluoroboron Dibenzoylmethane–Polylactide Nanoparticles in HeLa Cells

Janette Contreras,[†,§] Jiansong Xie,[†,§] Yin Jie Chen,[‡] Hua Pei,[†] Guoqing Zhang,[‡] Cassandra L. Fraser,[‡] and Sarah F. Hamm-Alvarez[†,*]

[†]Department of Pharmacology and Pharmaceutical Sciences, University of Southern California, Los Angeles, California 90033 and [‡]Department of Chemistry, University of Virginia, Charlottesville, Virginia 22904. [§]The first two authors contributed equally to the study.

ABSTRACT In this study, nanoparticles based on difluoroboron dibenzoylmethane–poly(lactic acid) (BF_2dbmPLA) are prepared. Polylactic acid or polylactide is a commonly used degradable polymer, while the boron dye possesses a large extinction coefficient, high emission quantum yield, two-photon absorption, and sensitivity to the surrounding environment. BF_2dbmPLA exhibits molecular-weight-dependent emission properties and can be formulated as stable nanoparticles, suggesting that its unique optical properties may be useful in multiple contexts for probing intracellular environments. Here we show that BF_2dbmPLA nanoparticles are internalized into cultured HeLa cells by endocytosis, and that within the cellular milieu, they retain their fluorescence properties. BF_2dbmPLA nanoparticles are photostable, resisting laser-induced photobleaching under conditions that destroy the fluorescence of a common photostable probe, LysoTracker Blue. Their endocytosis is also lipid-raft-dependent, as evidenced by their significant colocalization with cholera toxin B subunit in membrane compartments after uptake and their sensitivity of uptake to methyl-β-cyclodextrin. Additionally, BF_2dbmPLA nanoparticle endocytosis utilizes microtubules and actin filaments. Internalized BF_2dbmPLA nanoparticles do not accumulate in acidic late endosomes and lysosomes but within a perinuclear nonlysosomal compartment. These findings demonstrate the feasibility of using novel BF_2dbmPLA nanoparticles exhibiting diverse emission properties for *in situ*, live cell imaging and suggest that their endogenous uptake occurs through a lipid-raft-dependent endocytosis mechanism.

KEYWORDS: polylactide · fluorescence · imaging agent · endocytosis · lipid rafts · CLIC-GEEC

Light-emitting materials made by controlled synthetic methods and nanofabrication are useful for biological imaging and sensing. Versatile systems with easily controllable emission wavelengths are particularly desirable. Luminescent dye–polymer conjugates can be processed as nanoparticles and used to track intracellular structures and pathways.[1] Both fluorescence and phosphorescence emitters are widely used for these purposes. Phosphorescence is also useful for oxygen sensing, given sensitivity to oxygen quenching through triplet energy transfer.[2−4] For example, dual-emissive, boron biomaterial-based oxygen nanosensors are effective ratiometric tumor hypoxia imaging agents, with good spatial and temporal resolution.[5]

Here we prepared nanoparticles based on difluoroboron dibenzoylmethane–poly(lactic acid) or BF_2dbmPLA[6] and explored their potential as imaging agents for cellular uptake and trafficking studies. The constituent polymer, poly(lactic acid) (PLA) or polylactide, is commonly used as a sustainable packaging material and also is a key component of diverse biomedical devices such as bioresorbable sutures and implants, drug delivery systems, and tissue engineering matrices.[7] The boron dye, on the other hand, exhibits a large extinction coefficient, high emission quantum yield, two-photon absorption, and sensitivity to the surrounding environment, similar to nonpolymeric β-diketonate[8,9] and BODIPY[10] derivatives. Furthermore, in films and bulk materials, BF_2dbmPLA exhibits molecular weight (MW)-dependent luminescence as a single-component macromolecular system.[11]

To further assess the potential of this family of dye–polymer conjugates for biology, we investigated whether nanoparticles formed from BF_2dbmPLA[12] of different molecular weights retain color-tunable fluorescence in aqueous environments and within the cellular milieu. Previously, nanoparticles made from BF_2dbmPLA (M_n = 10 400 kDa) were investigated *in vitro*, and preliminary findings suggest that they accumulated in a perinuclear cellular compartment in Chinese hamster ovary (CHO) cells when they were added to the cell culture medium.[12] However, the optical properties

*Address correspondence to shalvar@usc.edu.

Received for review October 8, 2009 and accepted April 15, 2010.

Published online April 26, 2010.
10.1021/nn901385y

TABLE 1. Boron Nanoparticle Characterization Data

sample	M_n[a] (kDa)	PDI[b]	ε before[c] (M^{-1} cm^{-1})	ε after[d] (M^{-1} cm^{-1})	diameter[e] (nm)	PD[e]	λ_{em} F[f] (nm)	λ_{em} P[g] (nm)
BNP3	3.0	1.11	44900	42800	96	0.22	498	519
BNP6	6.0	1.08	38700	35600	88	0.22	442	509
BNP12	12.3	1.11	38300	36500	85	0.06	440	509
BNP17	16.8	1.21	37700	34900	77	0.14	439	508
BNP20	20.2	1.63	27700	25100	95	0.21	437	508

[a]Determined by GPC in THF *vs* polysytrene standards. [b]GPC PDI = polydispersity index. [c]BF_2dbmPLA extinction coefficient at λ_{max} = 396 nm in CH_2Cl_2, before nanoparticle fabrication. [d]As in footnote c for lyophilized samples after nanoparticle fabrication. [e]Determined by dynamic light scattering. PD = polydispersity. [f]Fluorescence emission maximum for aqueous nanoparticle suspension. [g]Phosphorescence emission maximum for aqueous nanoparticle suspension.

of boron nanoparticles (BNPs) made from polymers of different molecular weights have not been investigated in detail, either in aqueous suspension or in cells. This study characterizes the optical properties and stability of these BNPs, tests their internalization modalities in a HeLa fibroblast-like model cell line, and begins to determine their endogenous internalization mechanisms in this system. We show here that BNPs internalized into cultured cells retain their unique optical fluorescence emission properties and are photostable *in situ*. These BNPs exhibit equivalent internalization behavior regardless of the constituent polymer molecular weight within the ranges explored in this study. Finally, BNP internalization is rapid and occurs *via* a lipid-raft-dependent internalization pathway.

RESULTS AND DISCUSSION

Nanoparticle Fabrication and Characterization. Dibenzoylmethane (dbm) modified with a primary alcohol functionality was combined with BF_3 to synthesize BF_2dbmOH for use as an initiator in controlled, solvent-free, tin-catalyzed lactide polymerization, thus forming difluoroboron dibenzoylmethane−poly(lactic acid) (BF_2dbmPLA).[6] By changing reaction conditions (*e.g.*, monomer loading, polymerization times), boron polymers with different molecular weights were prepared.

Previously, experiments have shown that BF_2dbmPLA fluorescence emission spectra vary depending on the molecular weight of the polymer chain.[11] The MW dependence of BF_2dbmPLA fluorescence has been confirmed in powder and film states.

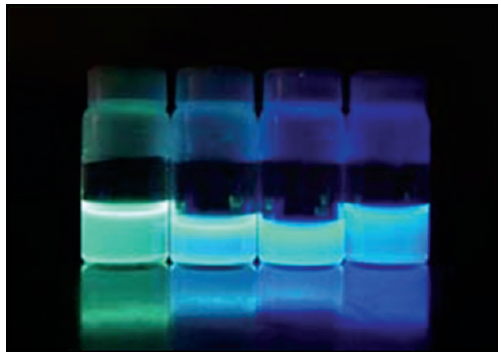

Figure 1. Image of BNP suspensions fabricated from polymers of different molecular weights (left to right, MW (kDa) = 3, 6, 13, 20) showing green to blue emission color tuning (λ_{ex} = 365 nm).

To further explore the potential of utilizing the optical properties of BF_2dbmPLA in biological imaging, sensing, and delivery systems and to test whether these unique color-tunable optical properties persist at the nanoscale and in aqueous environments, samples of various MWs were fabricated into nanoparticles *via* nanoprecipitation.[13,14] Characterization data are provided in Table 1. Samples are named as BNPX, where X is the molecular weight of the polymer used to fabricate the particles, 3, 6, 12, 17, and 20 kDa, respectively.

In the nanoparticle state, the molecular weight dependence of BF_2dbmPLA fluorescence is clearly evident upon visual inspection (Figure 1) and in emission spectra (Figure 2). Emission maxima, λ_{em}, range from 498 to 437 nm for nanoparticles composed of 3−20 kDa BF_2dbmPLA. This trend is likely caused by a dye concentration effect, induced by local polarity differences arising from fluorophore−fluorophore (F−F) interactions of different strengths. In nanoparticles made from lower MW BF_2dbmPLA (*e.g.*, BNP3), the fluorophores are in closer proximity and optical dipolar interactions are stronger. The excited state is stabilized, the energy gap between ground state and excited state is reduced, and emission is red-shifted. For nanoparticles made with high MW BF_2dbmPLA, in contrast, the stabilizing interaction is less, the energy gap between ground state and excited states is greater, and emission is blue-shifted. Under these conditions (*i.e.*, lower

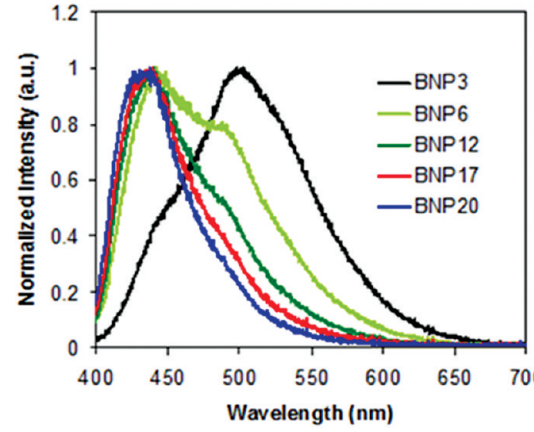

Figure 2. Fluorescence spectra of aqueous BNP suspensions (λ_{ex} = 365 nm).

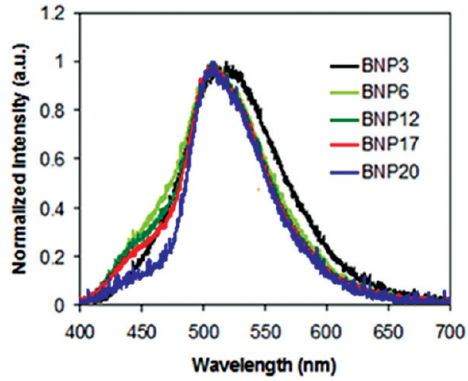

Figure 3. Delayed emission spectra for the BNP series. Delayed fluorescence (DF) (shoulder at λ ~ 440−465 nm) and room temperature phosphorescence (RTP) (λ ~ 508−519 nm) (λ_{ex} = 365 nm; ~500 ms delay).

dye/polymer loading), emission maxima parallel those observed in dilute solution.

BNPs, regardless of molecular weight, also exhibit room temperature phosphorescence (RTP). Delayed emission spectra were recorded with a ~500 ms delay after the black light excitation source was turned off. Gating allows for detection of long-lived (ms) RTP and delayed fluorescence (DF) after short-lived (ns) fluorescence has ceased (Figure 3). Delayed fluorescence results from thermal repopulation of the singlet state from the triplet excited state and appears as a high-energy shoulder (~440 nm) on the main RTP peak (~510−520 nm). The DF emission follows the same trend as fluorescence ($S_1 \rightarrow S_0$) and accounts for differences in the ~400−475 nm region of the emission spectra (Figures 2 and 3). It should be noted that BF_2dbmPLA phosphorescence is quenched in normoxic environments, and for the cellular uptake studies, we concentrate on the fluorescence properties of these nanoparticles, utilizing confocal and multiphoton fluorescence microscopy, flow cytometry, and fluorimetry.

The BNPs were also monitored over time to test for stability. After 11 weeks, the samples still exhibited MW-dependent fluorescence and RTP. Both the fluorescence and delayed emission spectra for the BNPs were essentially the same after 11 weeks as at the time of fabrication. After more than a year, fluorescence and phosphorescence are still present. These results suggest that these BNPs have good shelf life with respect to optical properties and may be exploited for longer term sensing applications.

Biological Studies. ***Internalization.*** It was previously shown that fluorescent BF_2dbmPLA nanoparticles could be detected intracellularly after a 1 h incubation in CHO cells.[12] To expand upon this initial observation, the intracellular distribution and emission spectra of BNPs were investigated in HeLa cells. Uptake experiments, where the cells were incubated with BNPs for 1 h and then analyzed by multiphoton fluorescence microscopy, showed that BNPs could be detected in the perinuclear region of the cells (Figure 4). A similar distribution pattern was observed across the range of MW

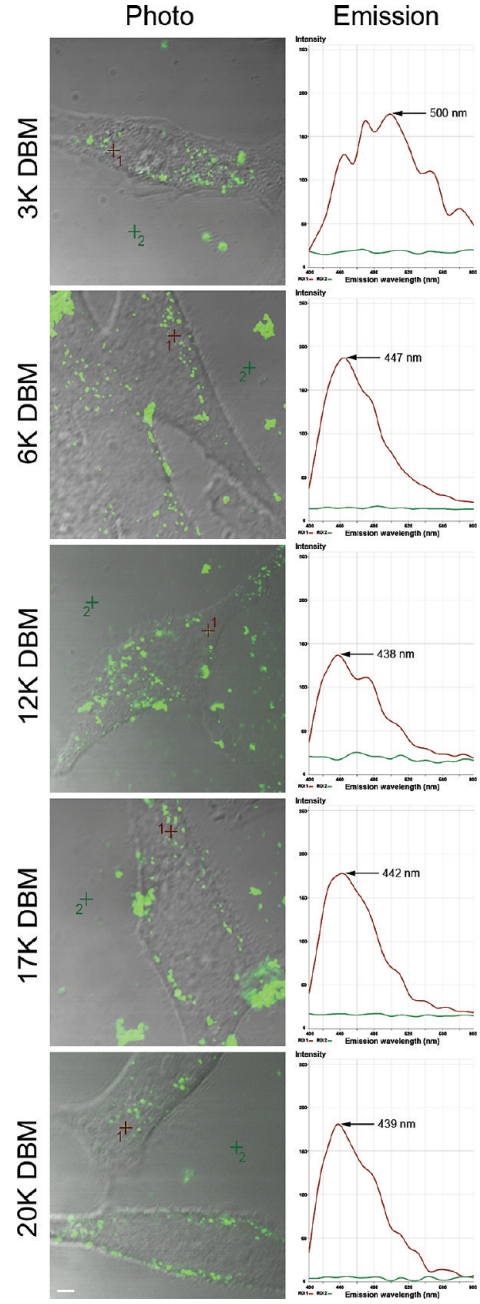

Figure 4. BNP distribution and intracellular emission spectra in HeLa cells. Left column: BNPs of different molecular weights show comparable punctate intracellular distributions in HeLa cells. HeLa cells were incubated with 200 μg/mL BNPs of different molecular weights for 1 h at 37 °C. After incubation, the BNPs were excited using the 790 nm line of a Chameleon multiphoton laser while emitted light was restricted in channel mode to a narrow range corresponding to the *in vitro* fluorescence emission spectrum of these particles, from 460 to 550 nm for BNP3 and from 420 to 485 nm for BNP6, BNP12, BNP17, and BNP20. Right column: BNPs were excited using the 790 nm line of a Chameleon multiphoton laser, and emission was calculated in lambda mode for acquisition of a spectral emission signal ranging from 400 to 600 nm. Spectra corresponding to the numbered points on the image to the left are shown on the right, with "1" denoting a region filled with a nanoparticle and "2" denoting background. Bar = 5 μm.

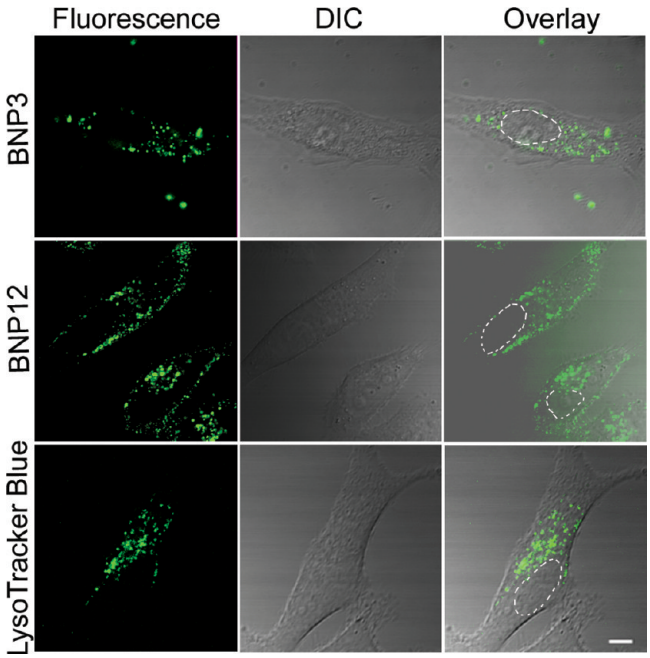

Figure 5. HeLa cell uptake of BNP3 and BNP12. HeLa cells were incubated with 200 μg/mL of BNP3 or BNP12 or with 2.5 μM LysoTracker Blue for 1 h at 37 °C and then imaged using confocal fluorescence microscopy. Excitation was at 790 nm for all markers. Emission was restricted to 460−550 nm for BNP3, 420−485 nm for BNP12, and 390−465 nm for LysoTracker Blue. Bar = 5 μm. Dotted lines represent the nuclear region identified from the DIC image.

used to make the nanoparticles. It should be noted that BNPs fabricated with different polymer MWs are comparable in size, in the range of 77−96 nm in diameter. Since size is a critical factor affecting the uptake of these nanoparticles, it is understandable that a similar uptake and distribution pattern was observed for the BNPs of different MW. As shown in Figure 4, the emission spectra for the internalized BNPs were very close to the fluorescence emission wavelengths reported in Table 1 for the corresponding molecular weights and remained distinct from one other. It should be noted that the particle excitation was provided by the 790 nm line of the multiphoton laser, showing the capability of these particles to exhibit multiphoton excitation and emission. This is particularly useful for *in vivo* applications that require the use of multiphoton excitation because of its greater ability to penetrate thicker sections or intact tissue. As an extension of these experiments, the uptake of two different nanoparticle samples, BNP3 and BNP12, was compared to a reference, UV-excitable fluorophore, LysoTracker Blue. This blue fluorescent dye, which labels highly acidic compartments within live cells and is enriched in lysosomal membranes, has an emission maxima of 422 nm. As shown in Figure 5, the intracellular distribution of BNP3 and BNP12 was quite similar to that of LysoTracker Blue, with all three showing significant perinuclear enrichment after 1 h uptake.

Photostability. The BNPs retain fluorescent and phosphorescent properties even after a year on the shelf under ambient light. To further explore their photostability, BNP3 and BNP12 (<1 month since fabrication) were exposed to direct UV light for up to 24 h, and the fluorescence intensity was measured both before and after exposure. The highly photostable LysoTracker Blue was used as a reference fluorophore. After direct UV light exposure for 24 h, approximately 50% of the fluorescence intensity of BNP3 and over 50% of BNP12 remained, while only 20−30% of the fluorescence intensity of LysoTracker Blue was detected (Figure 6A). The intracellular photostability of these nanoparticles was also examined. HeLa cells were incubated with either the highly photostable LysoTracker Blue or BNP (BNP3 or BNP12) for 1 h and were imaged over time during sequential bleaching. At the zero time point, the BNP fluorescence intensity exceeded that of LysoTracker Blue. After approximately 9.5 min of sequential bleaching, the LysoTracker Blue signal was almost completely photobleached, while the BNP12 signal was still readily detected (Figure 6B). Similar results were seen for BNP3 (data not shown). Because of the strong laser power required to conduct this experiment, we began to observe cell rounding and detachment consistent with cellular damage and death at time points preceding loss of BNP fluorescence. Since we could no longer focus on nanoparticles, which moved out of the focal plane as the cells detached, we were unable to continue this experiment. However, these studies do show that BNPs were highly photostable, more so than a highly photostable live cell commercial probe, and continuously up to conditions associated with cell damage/death due to high intensity illumination.

Internalization Mechanisms. To begin to understand BNP internalization mechanisms, as well as their intracellular trafficking patterns, we investigated their intracellular localization. LysoTracker Red is a fluorescent acidotrophic probe for tracking acidic organelles in live cells. HeLa cells were incubated with both BNP12 and LysoTracker Red simultaneously and then imaged. Little to no colocalization of BNP12 and LysoTracker Red was detected (Figure 7), suggesting that after 1 h the nanoparticles were not significantly localized to acidic compartments such as lysosomes, but rather to another perinuclear compartment. However, the distribution pattern in apparent membrane compartments confirmed an endocytic uptake mechanism. Because BNP fluorescence was poorly retained after the sample fixation and permeabilization necessary for use of immunofluorescence detection of specific compartment markers (data not shown), we were unable to determine the identity of this nonlysosomal perinuclear membrane compartment where BNPs accumulated. Imaging nanoparticles in fixed samples has historically been very challenging because nanoparticle fluorescence is often poorly retained after sample fixation and permeabilization.[15,16] Additionally, lack of potent mounting media for preserving initial and long-term

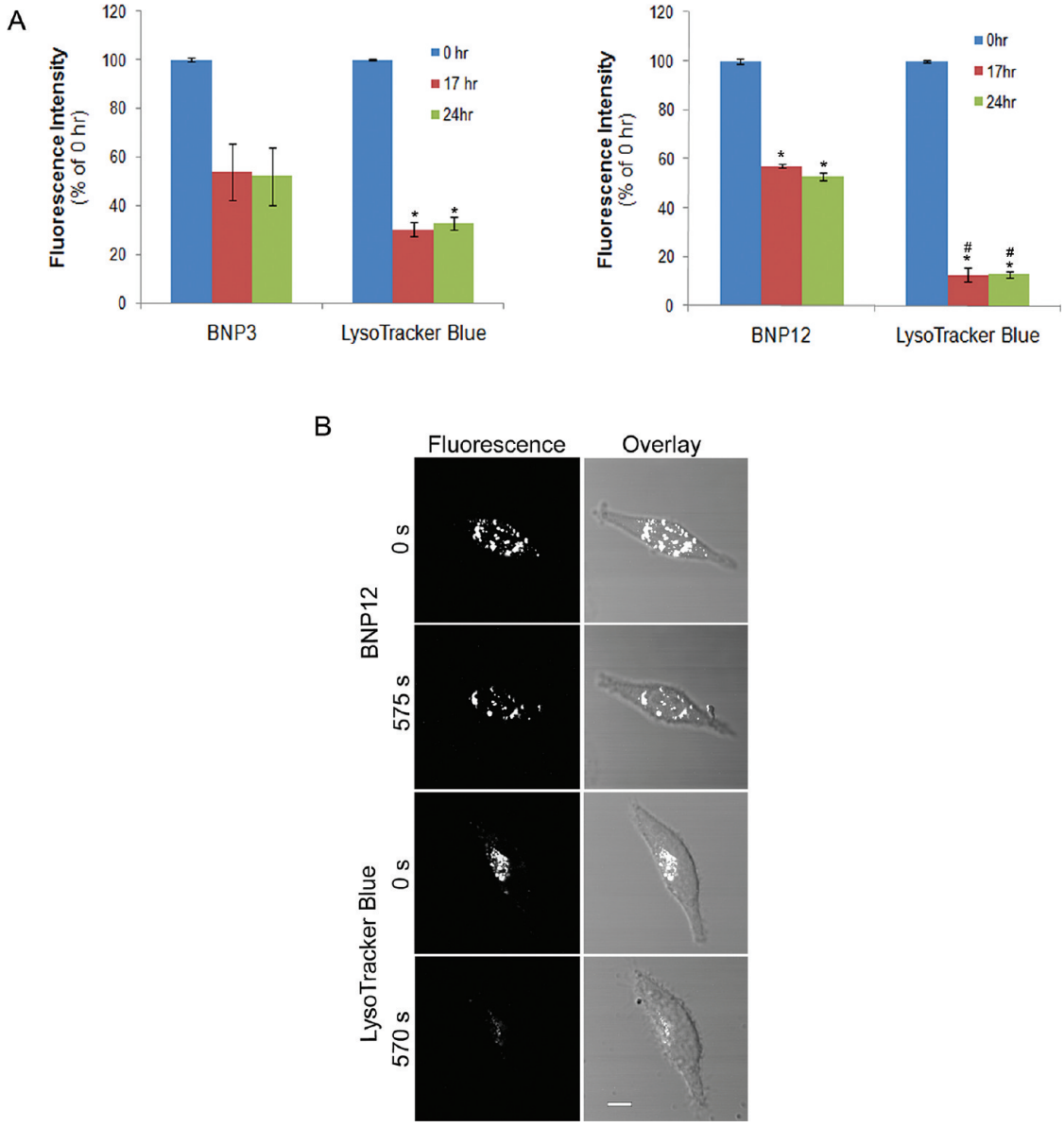

Figure 6. BNP photostability. (A) *In vitro* photostability. BNPs (5 μL of a 1 mg/mL stock) were added to a black, flat-bottomed 96-well plate, and the fluorescence intensity was measured at 0 h. Following exposure to direct UV light for 17 and 24 h, the fluorescence intensity was measured again as before. LysoTracker Blue was used as a reference UV-excitable fluorophore ($n = 3$ for both BNP3 and BNP12, * $p \leq 0.05$ relative to controls, and # $p \leq 0.05$ relative to BNP12). (B) *In vivo* photostability. HeLa cells seeded on glass-bottom culture dishes were incubated with either LysoTracker Blue or BNP12 and imaged over time as described in Methods. Bar = 5 μm.

fluorescence of the nanoparticles might contribute to the difficulties.

Endocytosis, the process by which internal membranes are produced by and detached from the plasma membrane lipid bilayer, can occur by multiple mechanisms. This process is critical for the ability of the cell, through regulation of its lipid and protein plasma membrane composition, to communicate with the extracellular environment.[17] It is equally important for modulating uptake and cellular sorting of extracellular soluble and plasma membrane-bound constituents, including nutrients, hormones, and extracellular particulates such as nanoparticle diagnostic probes or delivery devices, into the intracellular membrane system. Understanding the mechanisms of nanoparticle endocytosis is critical for development of these novel probes as therapeutic and diagnostic tools and for understanding how to optimize the use of a particular nanoparticle for a given situation.

For many years, the study of endocytosis has focused primarily on the pathway of clathrin-mediated endocytosis, an internalization mediated by association of adaptor proteins with the membrane, recruitment of a clathrin coat, and detachment of the clathrin-coated vesicle assisted by dynamin, a GTPase acting at the cytoplasmic face.[18−21] More recently, a plethora of additional mechanisms have emerged that use clathrin-independent pathways, which appear in fibroblast

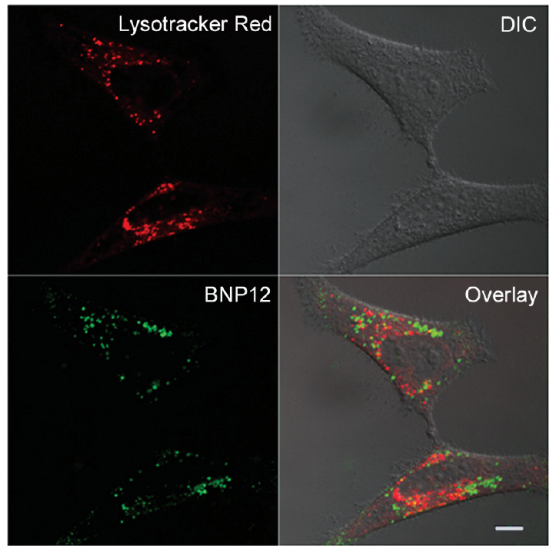

Figure 7. BNPs are not markedly colocalized with lysosomal compartments. HeLa cells were incubated with BNP12 (200 μg/mL) and LysoTracker Red for 1 h at 37 °C as described in Methods and then imaged. A UV laser was used for excitation of nanoparticles (green) and a HeNe1 laser for excitation of LysoTracker Red (red). Bar = 5 μm.

cells to be equally prevalent with clathrin-dependent pathways, and which include caveolar endocytosis, the clathrin-independent carrier GPI-AP-enriched early endosomal compartment (CLIC/GEEC) endocytosis, arf6-dependent endocytosis, flotillin-dependent endocytosis, and macropinocytosis. Many of these clathrin-independent pathways rely on the cholesterol-dependent clustering of lipid-anchored proteins into diverse microdomains.[22] The first of these lipid-raft-dependent pathways to be studied was the caveolar endocytosis pathway, which was thought to be mediated by flask-like invaginations coated with caveolin-1 detected on the internal plasma membrane of diverse cell types, including endothelial cells, and to involve detachment of caveolae from the plasma membrane by the protein, dynamin. It has now become clear that caveolae participate in internalization of only a few markers, while they appear to be able to also participate in formation of membrane extensions as well as regulation of other cellular processes.[18,22,23] Other mechanisms appear to account for the variety of other lipid-raft-dependent internalization mechanisms that are largely dynamin-independent and that have been detected in different systems.

For BNP uptake, several inhibitors were utilized to begin to discern the endocytic internalization mecha-

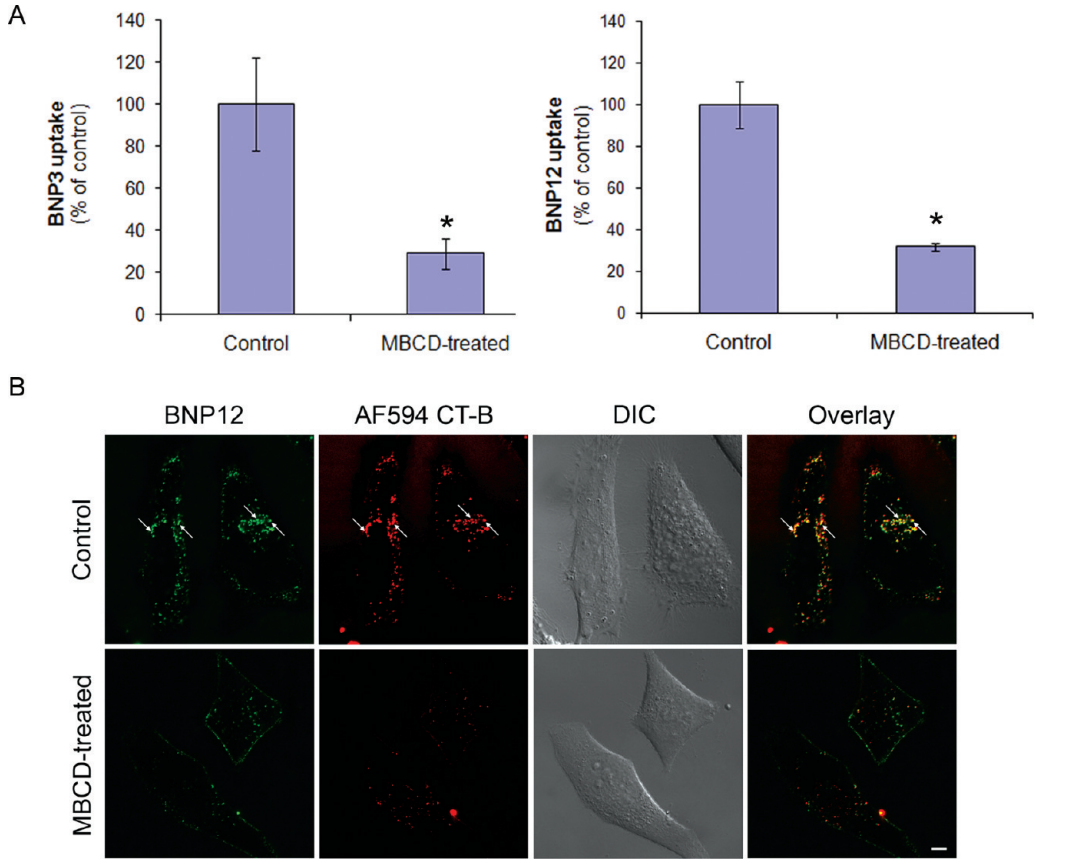

Figure 8. Uptake of BNPs is inhibited by MBCD treatment. (A) HeLa cells were untreated (control) or pretreated with 5 mM MBCD for 30 min at 37 °C prior to addition of BNP3 or BNP12 (200 μg/mL). Following uptake for 1 h at 37 °C, remaining surface-bound nanoparticles were removed by a mild acidic wash. The remaining cell-associated fluorescence signal was measured by flow cytometry using appropriate laser and filter settings ($n = 6$ for BNP3 and $n = 5$ for BNP12, * $p \leq 0.05$). (B) HeLa cells were incubated with 200 μg/mL BNP12 and 10 μg/mL Alexa Fluor 594-conjugated cholera toxin subunit B (AF594 CT-B) for 1 h at 37 °C with or without 5 mM MBCD pretreatment for 30 min at 37 °C. A UV laser was used for excitation of BNP12 (green) and a HeNe1 laser for excitation of AF594 CT-B. Arrows: colocalization of boron nanoparticles (BNP12) and AF594 CT-B. Bar = 5 μm.

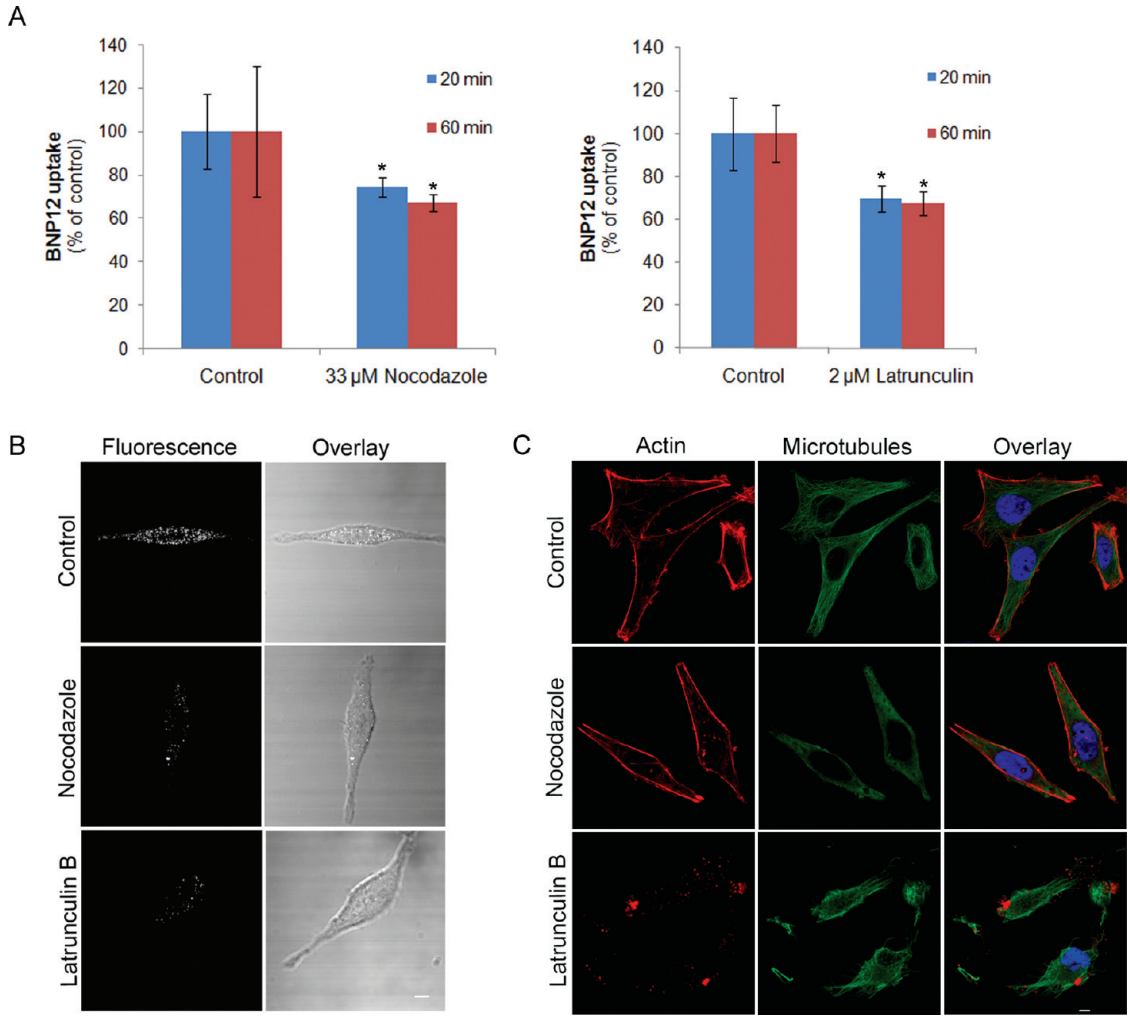

Figure 9. Disruption of the cytoskeleton affects BNP uptake. (A) HeLa cells were untreated (control) or pretreated with either 33 μM nocodazole or 2 μM Lat B prior to addition of BNP12 (200 μg/mL). Following uptake for 20 or 60 min at 37 °C, remaining surface-bound BNPs were removed by mild acid wash. The signal was collected by flow cytometry using appropriate laser and filter settings ($n = 8$ for 20 min and $n = 6$ for 60 min nocodazole; $n = 12$ for 20 min and $n = 14$ for 60 min Lat B. * $p \leq 0.05$). (B) HeLa cells were untreated (control) or pretreated with either 33 μM nocodazole or 2 μM Lat B prior to addition of BNP12 (200 μg/mL). Following uptake for 20 min at 37 °C, the cells were imaged using confocal laser microscopy. Excitation = 790 nm. Bar = 5 μm. (C) HeLa cells without any treatment (control) or treated with either 33 μM nocodazole or 2 μM Lat B for 60 min were fixed and labeled with a primary antibody to α-tubulin (green) combined with an appropriate secondary antibody in parallel with rhodamine−phalloidin to label actin (red). Bar = 5 μm.

nism. Because initial observations of rates of uptake as well as intracellular distribution suggested comparable behavior for all BNPs, we focused on BNP3 and BNP12 for detailed analysis of uptake mechanisms. The first inhibitor tested, methyl-*b*-cyclodextrin (MBCD), depletes cholesterol from the cell membranes, effectively inhibiting diverse cholesterol-dependent endocytic routes including caveolar endocytosis,[24,25] CLIC-GEEC endocytosis,[18] and, in some cases, even clathrin-mediated endocytosis.[18,26] HeLa cells pretreated with MBCD showed significantly reduced uptake of both BNP3 and BNP12 (Figure 8A) suggestive of uptake involving lipid rafts.

To determine additional features of BNP uptake through lipid-raft-dependent endocytosis, we utilized fluorescently labeled cholera toxin B (CT-B), which is known to be internalized *via* caveolar endocytosis and CLIC-GEEC.[18] Untreated and MBCD pretreated cells were incubated with BNP12 and Alexa Fluor 594-conjugated cholera toxin subunit B (AF594 CT-B). In control cells, BNP12 and AF594 CT-B were detected intracellularly with a significant amount of colocalization. In contrast, cells pretreated with MBCD showed reduced uptake of both BNP12 and AF594 CT-B (Figure 8B).

To try to distinguish between caveolar-dependent internalization of BNP *versus* their internalization *via* other lipid-raft-dependent mechanisms, we utilized dynasore, an inhibitor of dynamin which is thought to participate in both clathrin-mediated and caveolar endocytic mechanisms.[18] While dynasore did not consistently impair BNP nor CT-B uptake in HeLa cells (at doses comparable to those previously used in other HeLa cells[27−30]), its effects on a control

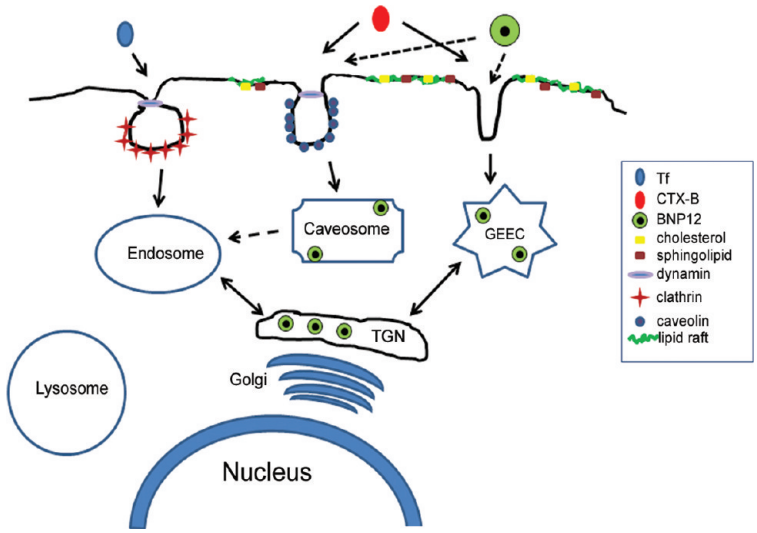

Figure 10. Schematic diagram depicting BNP uptake through lipid-raft-dependent internalization pathways that also serve as the routes of uptake for cholera toxin B (CT-B). The BNPs may ultimately reach the perinuclear trans-Golgi network (TGN) by one of two pathways. The first is by direct communication between the GPI-AP-enriched early endosomal compartment (GEEC) and the TGN. The second is by communication between caveosomes and classical endosomes and subsequent communication between the latter and the TGN.

ligand, Texas Red-EGF, which is known to use dynamin-dependent clathrin-mediated endocytosis,[31] also showed little to no effects (data not shown). This finding suggested that dynasore was not acting as a reliable dynamin inhibitor under these conditions in the HeLa cells.

These data suggest that BNP uptake is dependent upon lipid rafts. Cholesterol depletion would be expected to affect multiple lipid-raft-dependent endocytic pathways including caveolar endocytosis, CLIC/GEEC endocytosis, and flotillin endocytosis. It has been established that CT-B traffics through both caveolar and CLIC/GEEC pathways; since it is significantly colocalized with BNP, this suggests that these nanoparticles utilize similar internalization pathways. Furthermore, CT-B has been shown to traffic directly from a peripheral tubular intermediate to the Golgi apparatus.[18,24] Our finding that BNPs colocalize with CT-B in a perinuclear compartment that is not labeled with the acidic organelle probe, LysoTracker, suggests that these particles, like many pathogens, may be able to exploit endogenous internalization pathways.

Role of the Cytoskeleton. Actin filaments have been implicated in various capacities in diverse endocytic pathways including caveolar and CLIC/GEEC-mediated endocytosis.[18,32] Microtubules are less commonly associated with initial endocytic uptake processes but have been reported to play an important role in the sorting of endocytosed materials within endosomal compartments, in concert with motor proteins.[33,34] We examined the effects of nocodazole and latrunculin B (Lat B) on BNP uptake. Both agents disrupt the cell cytoskeleton and, by extension, events requiring participation by these filament systems: nocodazole is an established inhibitor of the microtubule network, promoting microtubule disassembly,[33] while Lat B is an inhibitor of actin filament assembly.[35] Both agents have previously been used successfully in HeLa cells.[36−38] HeLa cells pretreated with either nocodazole or Lat B showed significantly reduced uptake of BNP12 with effects readily detectable by 20 min (Figure 9A,B)). Comparable results were seen at 60 min, although the effect was less pronounced for nocodazole (data not shown). Analysis of microtubule and microfilament organization in HeLa cells treated with nocodazole or Lat B confirmed the expected disassembly of microtubules and microfilaments, respectively (Figure 9C).

While quantitative evaluation of particle uptake revealed an approximate 40% inhibition of internalization, evaluation of individual cells treated with nocodazole or Lat B suggested an even more potent inhibition. Actin filament disassembly might impact diverse endocytic pathways including caveolar or CLIC/GEEC-mediated endocytosis, consistent with the possibility of internalization *via* this pathway. Microtubules are more commonly associated with endosomal and post-endosomal sorting processes as well as maintenance of unique compartment morphologies;[39,40] their disassembly by nocodazole might affect the dynamics of intracellular sorting, thus increasing the efficiency of recycling through impairment of post-endocytic processing.

The abundance of nanoparticle formulations, sizes, shapes, and compositions has provided a series of hurdles to the comprehensive understanding of their uptake properties.[41] Consensus exists in the literature about the features of nanoparticles that are important for their uptake: size and surface charge.[42−46] While the specific effects of size and surface charge are debatable, it has been shown that nanoparticles with positive surface charge are generally more readily endocytosed because of their affinity for the negatively charged plasma membrane.[46,47] The use of common cationic liposomal formulations, essentially primitive nanoparticles, for efficient cell transfection lends credence to this observation.[47,48] However, it has been reported that endocytosis of cationic liposomes is significantly reduced in cells enriched in lipid raft markers such as GM-1,[49] suggesting that lipid raft domains may have an underlying preference for negatively charged nanoparticles. Since the BNPs studied here are likely negatively charged (based on the inclusion of PLA which is known to form a negatively charged nanoparticle[44]) and appear to be internalized using lipid-raft-dependent processes, this suggests the need for further study of the factors governing charge interaction at lipid rafts. A schematic representation of their internalization pathway is depicted in Figure 10.

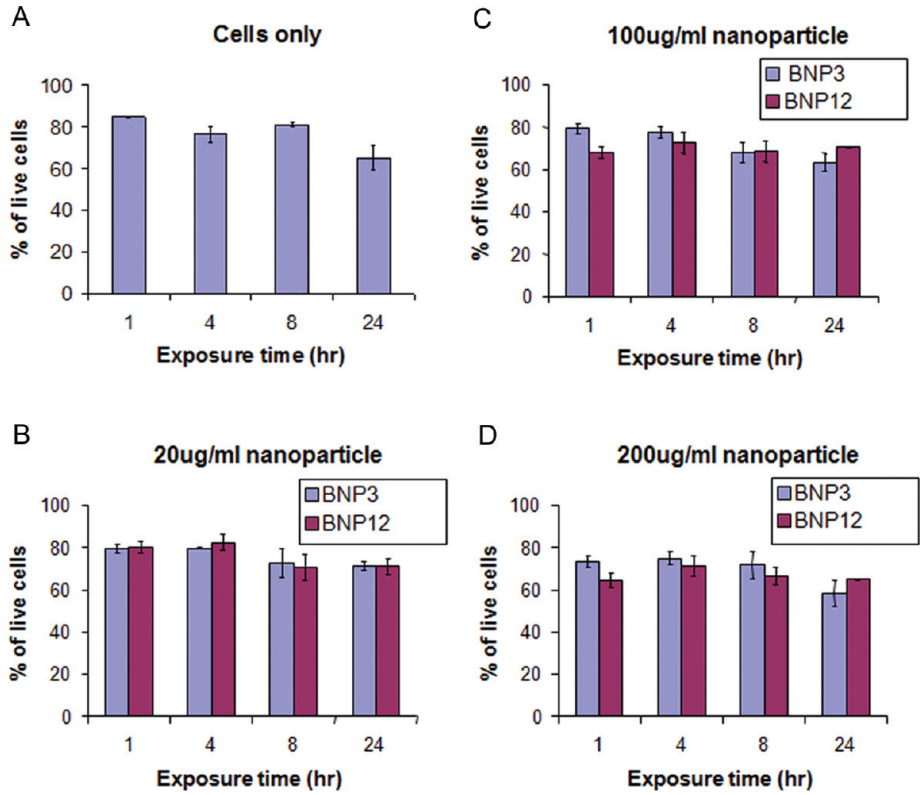

Figure 11. BNP exposure does not affect cell viability. HeLa cells were exposed to culture medium (A), 20 μg/mL (B), 100 μg/mL (C), or 200 μg/mL (D) of BNP3 or BNP12 for various time periods up to 24 h at 37 °C. Cell viability was assayed using a LIVE/DEAD viability/cytotoxicity kit (n = 3).

Nanoparticle endocytosis can occur in a variety of ways. In fact, a single type of nanoparticle can employ multiple endocytic routes depending on its size. For example, carboxyl-modified fluorescent polystyrene nanoparticles that are 24 nm in diameter were able to enter HeLa cells *via* a nonclassical (clathrin-, caveolin-, and cholesterol-independent) pathway, while equivalently composed 43 nm nanoparticles entered cells predominantly *via* clathrin-mediated endocytosis.[50] PLA and polylactide−polyglycolide (PLGA) nanoparticles have been shown to enter vascular smooth muscle cells through a combination of fluid phase pinocytosis and clathrin-mediated endocytosis.[44,51,52] Cationic poly(ethylene glycol)(PEG)−PLA nanoparticles also use the clathrin-mediated pathway in HeLa cells, whereas anionic PEG−PLA nanoparticles do not.[53] Polystyrene nanoparticles appear to translocate across rat alveolar epithelial cell monolayers by an endocytosis-independent, transcellular pathway.[54] Other factors that may influence endocytosis of nanoparticles are their formulation and surface group modifications. It is generally assumed that the addition of one or more targeting moieties may facilitate retargeting of the core nanoparticle away from the default pathway and to a new one, depending on the efficiency of coating of the targeting moiety, its accessibility to the targeted receptor, the strength of the interaction, and the abundance of the targeted receptor.[14,46,53,55] The findings on BNPs thus far suggest that BNPs composed of the different MW polymers tested here may utilize similar trafficking pathways, suggesting that the features that dominate their behavior are associated with the surface characteristics of the particle rather than the small variations in particle size. Finally, nanoparticle internalization characteristics may vary depending upon whether the cells are transformed (like HeLa cells), or not, and may also vary with the cell cycle. Our work has focused on assessment of internalization in nondividing, subconfluent but unsynchronized cells, but future analyses which compare the pathways in different states of the cell cycle may be of great interest.

Cytotoxicity Assessment. Among the potential applications for use of biodegradable nanoparticles are biological imaging and sensing. For this reason, it was important that the cytotoxicity be evaluated. HeLa cells were exposed to various doses of BNP3 or BNP12 for various time periods, and their viability was assayed using a viability/cytotoxicity kit. Approximately 60% of the cells incubated with BNPs were viable after 24 h of exposure, comparable to control cells not exposed to BNPs (Figure 11). Viability was reduced to ~60% in control cells due to the absence of serum, which we omitted in these studies so as to make the cytotoxicity assays comparable to those used for analysis of BNP uptake. These data suggest that the BNPs are not acutely cytotoxic.

CONCLUSION

The first steps in demonstrating biological utility for a new nanoparticle formulation are the characteriza-

tion of its properties when in biological environment(s) of interest, as well as the characterization of its interactions with this environment. The unique optical properties of nanoparticles must be sustainable within a biological milieu to be useful for biomedical diagnostic applications. Here we have demonstrated that the unique and photostable emission properties of BF_2dbmPLA nanoparticles are discernible both in aqueous solution and *in situ* in live cells using multiphoton excitation. We have also shown the selective endocytosis of BNPs, through a specific mechanism, and the ability of the cells to tolerate high doses of BNPs for up to 24 h in culture. These studies, collectively, suggest that BNPs are useful, nontoxic agents for further development in the investigation of intracellular environments and trafficking pathways.

The next step in characterization of the endogenous internalization mechanism in these fibroblastic cells will logically involve utilization of molecular constructs allowing manipulation of different effector pathways and assessment of colocalization of BNPs *in situ* with additional live cell membrane compartment markers. Likewise, investigation of the dynamics of BNP trafficking within cells expressing fluorescent tubulin and actin will enable visualization of intracellular movement in real time with respect to other membrane and structural markers. An equally important question that remains to be addressed is whether BNPs can be successfully redirected from their default pathway, characterized here in HeLa cells, to other endocytic pathways so as to expand their potential utility as probes. Utilization of the unique optical properties of BNPs would ideally involve the attachment of targeting ligands, which may direct these moieties to diverse intracellular environments, as probes to explore microenvironments and their dynamic properties, including local oxygen concentrations and ways that they change over time. Another attractive application of the bright, color-tunable BNPs is that conjugating the BNPs of different molecular weights to different ligands of interest would enable the performance of multiplex studies.

Since no toxicity has been reported at high doses of BNPs in cultured cells, these particles exhibit characteristics *in vitro* that may be preferable relative to alternative nanoparticles such as quantum dots, whose core structure is relatively more toxic, and toxicity is generally poorly studied.[56,57] For example, BNPs are two-photon excitable, bright, and also degradable. These properties are particularly useful for *in vivo* applications. The relative ease of preparation and cost effectiveness suggest great value in the further investigation and application of BNPs in diverse *in vitro* and *in vivo* situations which require photostable, inexpensive, and modifiable nanoparticles to probe diverse environments. The demonstration that they are excitable using multiphoton excitation, also in this study, extends their applicability into animal models and even into the clinical setting.

METHODS

Reagents. 3,6-Dimethyl-1,4-dioxane-2,5-dione (D,L-lactide, Aldrich) was recrystallized twice from ethyl acetate and stored under nitrogen. Solvents, CH_2Cl_2 and THF, were dried and purified by passing through alumina columns. Tin(II) 2-ethylhexanoate ($Sn(oct)_2$, Spectrum), boron trifluoride diethyl etherate (Aldrich, purified, redistilled), and all other reagents and solvents were used as received without further purification. DbmOH,[58] BF_2dbmOH,[6] and BF_2dbmPLA[6] samples of different molecular weights[11] were prepared as previously reported. Dialysis tubing (Spectrum, volume/length = 6.4 mL/cm, MWCO = 12−14 000) was washed and soaked in distilled H_2O overnight before use. Nanoparticles were fabricated as previously described.[12] Methyl-β-cyclodextrin (MBCD) was purchased from Sigma-Aldrich. Texas Red-EGF (TR-EGF), LysoTracker Red DND-99, LysoTracker Blue DND-22, AF594 cholera toxin B, nocodazole, and the LIVE/DEAD viability/cytotoxicity kit for mammalian cells were all purchased from Invitrogen. Latrunculin B (Lat B) was purchased from Calbiochem.

Characterization of Nanoparticles. UV/vis spectra were recorded on a Hewlett-Packard 8452A diode-array spectrophotometer. Molecular weights were determined by GPC (THF, 20 °C, 1.0 mL/min) *versus* polystyrene standards with RI and UV/vis detection (λ = 396 nm for BF_2dbmPLA), and a correction factor of 0.58 was applied to all data, as previously described.[4] Polymer Laboratories 5 μm mixed-C columns along with Hewlett-Packard instrumentation (Series 1100 HPLC) and Viscotek software (TriSEC GPC Version 3.0, Viscotek Corp) were used in the GPC/RI or GPC/UV analysis. Nanoparticle sizes were determined by dynamic light scattering (DLS) (90° angle) on the Photocor Complex (Photocor Instruments Inc., USA) equipped with a He−Ne laser (Coherent, USA, Model 31-2082, 632.8 nm, 10 mW). Size and polydispersity analyses were performed using DynaLS software (Alango, Israel). The suspension was analyzed as such or diluted (0.5 mL) in H_2O (9.5 mL). Photographs of nanoparticles were taken in the dark using a Casio Exilim Zoom EX-Z850 camera with the automatic setting (no flash).

Acquisition of Luminescence Spectra. Emission spectra for the BNP suspensions were recorded with an Ocean Optics USB2000 fiber optic spectrometer after excitation with a hand-held UV lamp (λ_{ex} = 365 nm; long wavelength setting). A ~500 ms delay was employed in collecting delayed emission spectra (*i.e.*, delayed fluorescence and phosphorescence).

Cell Culture. HeLa cells were obtained from the American Type Culture Collection (ATCC) and were cultured in a humidified incubator at 37 °C in 95% air/5% CO_2 in phenol-red-free Dulbecco's modified essential medium (DMEM) (4.5 g/L glucose with 10% FBS, 1% glutamine, and 1% nonessential amino acids) and split with trypsin/EDTA as recommended by the manufacturer. Cells were routinely analyzed at low passage in the subconfluent state, although they were not synchronized.

Photostability Assays. For measurement of *in vitro* photostability, different BNPs were assayed using a black flat-bottomed 96-well plate. BNPs were added dropwise (5 μL of a 1 mg/mL stock) into 195 μL room temperature incubation buffer (phenol-red-free, serum-free DMEM with 1% penicillin/streptomycin and 20 mM HEPES). Serum was omitted from the incubation buffer to prevent possible nanoparticle aggregation. LysoTracker Blue was used as a reference for a UV-excitable and photostable fluorophore (5 μL of a 1 mM stock). Fluorescence intensity was measured at 0 h using an Envision 2103 Multilabel Reader (Perkin-Elmer, excitation filter = 340 nm, emission filter = 460 nm). The plate was exposed to direct UV light for 17 or 24 h and the fluo-

rescence intensity measured again as before. For *in vivo* photostability studies, HeLa cells were seeded on 35 mm glass-bottomed culture dishes at a density of 8.5×10^4 cells/dish. On day 2 of culture, the cells were rinsed once with PBS and the medium was replaced with cold incubation buffer of the composition described above (800 μL). BNPs were added dropwise (200 μL) and incubated at 4 °C for 1 h. Unbound BNPs were rinsed off gently using PBS, the incubation buffer was replaced (1 mL), and the cells were incubated at 37 °C for 1 h. For reference, LysoTracker Blue (2.5 μM final concentration) was added to cells after initial rinse, and the cells were incubated at 37 °C for 1 h. Following the 37 °C incubation, the cells were rinsed four times with PBS and imaged. The BNPs or LysoTracker Blue were imaged using time series sequential bleach settings. For each cycle, the image was acquired using a line 4 average, which was followed by 10 iterations of bleaching using the 790 nm line at 4% power (74 mW). Bleaching was started after one scan and repeated after one scan. Time-lapse imaging was performed using a Zeiss LSM 510 Meta NLO imaging system equipped with a Chameleon multiphoton laser mounted on a vibration-free table.

Uptake Assays. HeLa cells were seeded on 6-well plates at a density of 1.5×10^5 cells/well. On day 2 of culture, cells were rinsed briefly with phosphate-buffered saline (PBS) containing 1 mM $CaCl_2$ and 0.5 mM $MgCl_2$ and the media replaced with incubation buffer (900 μL) with or without MBCD (5 mM) or Lat B (2 μM) and incubated at 37 °C for 30 min. After cooling on ice for 10 min, BNPs (100 μL) were added dropwise and incubated at 4 °C for 1 h. For nocodazole pretreatment, 33 μM nocodazole was added prior to incubation at 4 °C. Unbound BNPs were rinsed off with a gentle PBS ($+Ca^{2+}$, $+Mg^{2+}$) wash, the incubation buffer was replaced, and the cells were warmed to 37 °C for various times up to 1 h. After incubation, the cells were incubated with an ice-cold mild acidic wash buffer (0.1 M sodium acetate, 0.05 M NaCl, pH 5.5) for 10 min at 4 °C. Following the acid wash, the cells were washed three times with ice-cold PBS ($+Ca^{2+}$, $+Mg^{2+}$). To collect the cells, 700 μL of trypsin (37 °C) was added to each well and incubated at 37 °C for 3 min. The cells were then transferred to 1.5 mL Eppendorf tubes and centrifuged for 5 min at 800 rpm at 4 °C. The cell pellet was resuspended in 0.5 mL of ice-cold PBS (without Ca^{2+} or Mg^{2+}) and filtered through a 70 μm nylon filter, and the fluorescence intensity was measured by flow cytometry.

Confocal and Multiphoton Fluorescence Microscopy. For BNP uptake studies, HeLa cells were seeded on 35 mm glass-bottomed culture dishes at a density of 8.5×10^4 cells/dish. On day 2 of culture, the cells were rinsed with PBS prior to addition of BNPs dropwise (200 μL) with incubation at 4 °C for 1 h. Unbound BNPs were rinsed off with a gentle PBS wash, the incubation buffer was replaced, and the cells were warmed to 37 °C for various times up to 4 h in the absence or presence of treatments. After incubation, the cells were rinsed four times with PBS and imaged with a Zeiss LSM 510 Meta NLO imaging system equipped with a Coherent Chameleon multiphoton laser mounted on a vibration-free table. For most studies, BNPs were excited in intact cells using the 790 nm line of the multiphoton laser. For assessment of colocalization of BNP and LysoTracker Red or AF594 cholera toxin B in live cells, we utilized a Zeiss LSM 510 confocal microscope equipped with UV, argon, and green HeNe lasers for confocal fluorescence microscopy. For MBCD or Lat B pretreatment, 5 mM MBCD or 2 μM Lat B was added for 30 min at 37 °C prior to addition of BNPs. For nocodazole treatment, 33 μM nocodazole was added with the BNPs prior to incubation at 4 °C. For colocalization studies, LysoTracker Red (50 nM), AF594 cholera toxin B (10 μg/mL), or TR-EGF (200 ng/mL) was added to cells prior to incubation at 37 °C. For immunostaining, following treatment with either 33 μM nocodazole or 2 μM Lat B, the cells were fixed in 4% paraformaldehyde prior to the addition of mouse monoclonal antibody to α-tubulin and appropriate secondary fluorophore-conjugated antibody.

Cytotoxicity Assays. HeLa cells were seeded on 96-well plates at a density of 8×10^3 cells/well. On day 1 of culture, the cells were rinsed briefly in 200 μL of ice-cold PBS ($+Ca^{2+}$, $+Mg^{2+}$). Varying concentrations of BNPs (20−200 μg/mL) in incubation buffer (phenol-red-free, serum-free DMEM with 1% P/S and 20 mM HEPES) were added dropwise (200 μL total volume) and incubated on ice for 1 h. Following the incubation, the cells were washed once in 200 μL of ice-cold PBS ($+Ca^{2+}$, $+Mg^{2+}$), the media replaced with 200 μL of 37 °C incubation buffer, and the plate was incubated at 37 °C for various time points (1−24 h). Calcein (494/517 nm) and ethidium homodimer-1 (528/617 nm) provided in the LIVE/DEAD cell assay kit (Invitrogen) were used to detect live/dead cells and were added to cells after the incubation (50 μL of 0.5 μM calcein AM and 1.5 μM EthD-1). Fluorescence intensity was measured using an Envision 2103 Multilabel Reader (Perkin-Elmer).

Statistics. Cells from each experiment were analyzed individually, and the results from different experiments were compared using the Student's *t*-test with $p \leq 0.05$ to evaluate the statistical significance of any observed changes.

Acknowledgment. We thank the National Science Foundation (BES 0402212, CHE-0718879 to C.L.F.), the UVA nanoSTAR Institute (seed grant to C.L.F.), the UVA Cancer Center (NCI Cancer Center Support Grant P30 CA4459 and James and Rebecca Craig Foundation to C.L.F), and the National Institutes of Health (RO1 EY017293 to S.F.H.-A.) for support for this work. We also thank the USC Center for Liver Diseases (P30 DK048522) for access to the Cell Biology Core Facility. We gratefully acknowledge the Harrison Undergraduate Research Program at UVA for a research award to Y.J.C. and the National Institutes of Health for a Ruth Kirchstein Predoctoral Fellowship for J.C. (F31EY018807).

Supporting Information Available: Supplemental figure shows time course uptake data for BNP12. This material is available free of charge *via* the Internet at http://pubs.acs.org.

REFERENCES AND NOTES

1. Torchilin, V. P. Fluorescence Microscopy To Follow the Targeting of Liposomes and Micelles to Cells and Their Intracellular Fate. *Adv. Drug Delivery Rev.* **2005**, *57*, 95–109.
2. Cochran, D. M.; Fukumura, D.; Ancukiewicz, M.; Carmeliet, P.; Jain, R. K. Evolution of Oxygen and Glucose Concentration Profiles in a Tissue-Mimetic Culture System of Embryonic Stem Cells. *Ann. Biomed. Eng.* **2006**, *34*, 1247–1258.
3. Sanchez, J. M.; Sacks, R. D. Development of a Multibed Sorption Trap, Comprehensive Two-Dimensional Gas Chromatography, and Time-of-Flight Mass Spectrometry System for the Analysis of Volatile Organic Compounds in Human Breath. *Anal. Chem.* **2006**, *78*, 3046–3054.
4. Vanderkooi, J. M.; Maniara, G.; Green, T. J.; Wilson, D. F. An Optical Method for Measurement of Dioxygen Concentration Based Upon Quenching of Phosphorescence. *J. Biol. Chem.* **1987**, *262*, 5476–5482.
5. Zhang, G.; Palmer, G. M.; Dewhirst, M. W.; Fraser, C. L. A Dual-Emissive-Materials Design Concept Enables Tumour Hypoxia Imaging. *Nat. Mater.* **2009**, *8*, 747–751.
6. Zhang, G.; Chen, J.; Payne, S. J.; Kooi, S. E.; Demas, J. N.; Fraser, C. L. Multi-Emissive Difluoroboron Dibenzoylmethane Polylactide Exhibiting Intense Fluorescence and Oxygen-Sensitive Room-Temperature Phosphorescence. *J. Am. Chem. Soc.* **2007**, *129*, 8942–8943.
7. Griffith, L. G.; Naughton, G. Tissue Engineering—Current Challenges and Expanding Opportunities. *Science* **2002**, *295*, 1009–1014.
8. Chow, Y. L.; Johansson, C. I.; Zhang, Y. H.; Gautron, R.; Yang, L.; Rassat, A.; Yang, S. Z. Spectroscopic and Electrochemical Properties of 1,3-Diketonatoboron Derivatives. *J. Phys. Org. Chem.* **1996**, *9*, 7–16.
9. Cogné-Laage, E.; Allemand, J. F.; Ruel, O.; Baudin, J. B.; Croquette, V.; Blanchard-Desce, M.; Jullien, L. Diaroyl(methanato)boron Difluoride Compounds as Medium-Sensitive Two-Photon Fluorescent Probes. *Chemistry* **2004**, *10*, 1445–1455.
10. Loudet, A.; Burgess, K. BODIPY Dyes and Their Derivatives: Syntheses and Spectroscopic Properties. *Chem. Rev.* **2007**, *107*, 4891–4932.
11. Zhang, G.; Kooi, S. E.; Demas, J. N.; Fraser, C. L. Emission Color Tuning with Polymer Molecular Weight for

Difluoroboron Dibenzoylmethane-Polylactide. *Adv. Mater.* **2008**, *20*, 2099–2104.
12. Pfister, A.; Zhang, G.; Zareno, J.; Horwitz, A. F.; Fraser, C. L. Boron Polylactide Nanoparticles Exhibiting Fluorescence and Phosphorescence in Aqueous Medium. *ACS Nano* **2008**, *2*, 1252–1258.
13. Farokhzad, O. C.; Langer, R. Nanomedicine: Developing Smarter Therapeutic and Diagnostic Modalities. *Adv. Drug Delivery Rev.* **2006**, *58*, 1456–1459.
14. Whitesides, G. M. Nanoscience, Nanotechnology, and Chemistry. *Small* **2005**, *1*, 172–179.
15. Buono, C.; Anzinger, J. J.; Amar, M.; Kruth, H. S. Fluorescent Pegylated Nanoparticles Demonstrate Fluid-Phase Pinocytosis by Macrophages in Mouse Atherosclerotic Lesions. *J. Clin. Invest.* **2009**, *119*, 1373–1381.
16. Williams, Y.; Byrne, S.; Bashir, M.; Davies, A.; Whelan, A.; Gun'ko, Y.; Kelleher, D.; Volkov, Y. Comparison of Three Cell Fixation Methods for High Content Analysis Assays Utilizing Quantum Dots. *J. Microsc.* **2008**, *232*, 91–98.
17. Conner, S. D.; Schmid, S. L. Regulated Portals of Entry into the Cell. *Nature* **2003**, *422*, 37–44.
18. Doherty, G. J.; McMahon, H. T. Mechanisms of Endocytosis. *Annu. Rev. Biochem.* **2009**, *78*, 857–902.
19. Kirchhausen, T.; Macia, E.; Pelish, H. E. Use of Dynasore, the Small Molecule Inhibitor of Dynamin, in the Regulation of Endocytosis. *Methods Enzymol.* **2008**, *438*, 77–93.
20. Macia, E.; Ehrlich, M.; Massol, R.; Boucrot, E.; Brunner, C.; Kirchhausen, T. Dynasore, a Cell-Permeable Inhibitor of Dynamin. *Dev. Cell* **2006**, *10*, 839–850.
21. Thompson, H. M.; McNiven, M. A. Discovery of a New 'Dynasore'. *Nat. Chem. Biol.* **2006**, *2*, 355–356.
22. Kirkham, M.; Parton, R. G. Clathrin-Independent Endocytosis: New Insights into Caveolae and Non-Caveolar Lipid Raft Carriers. *Biochim. Biophys. Acta* **2005**, *1745*, 273–286.
23. Kiss, A. L.; Botos, E. Endocytosis *via* Caveolae: Alternative Pathway with Distinct Cellular Compartments To Avoid Lysosomal Degradation. *J. Cell. Mol. Med.* **2009**, *13*, 1228–1237.
24. Le, P. U.; Nabi, I. R. Distinct Caveolae-Mediated Endocytic Pathways Target the Golgi Apparatus and the Endoplasmic Reticulum. *J. Cell. Sci.* **2003**, *116*, 1059–1071.
25. Parton, R. G.; Simons, K. The Multiple Faces of Caveolae. *Nat. Rev. Mol. Cell Biol.* **2007**, *8*, 185–194.
26. Rodal, S. K.; Skretting, G.; Garred, O.; Vilhardt, F.; van Deurs, B.; Sandvig, K. Extraction of Cholesterol with Methyl-β-Cyclodextrin Perturbs Formation of Clathrin-Coated Endocytic Vesicles. *Mol. Biol. Cell* **1999**, *10*, 961–974.
27. Abban, C. Y.; Bradbury, N. A.; Meneses, P. I. HPV16 and BPV1 Infection Can Be Blocked by the Dynamin Inhibitor Dynasore. *Am. J. Ther.* **2008**, *15*, 304–311.
28. Dausend, J.; Musyanovych, A.; Dass, M.; Walther, P.; Schrezenmeier, H.; Landfester, K.; Mailander, V. Uptake Mechanism of Oppositely Charged Fluorescent Nanoparticles in HeLa Cells. *Macromol. Biosci.* **2008**, *8*, 1135–1143.
29. Huang, F.; Khvorova, A.; Marshall, W.; Sorkin, A. Analysis of Clathrin-Mediated Endocytosis of Epidermal Growth Factor Receptor by RNA Interference. *J. Biol. Chem.* **2004**, *279*, 16657–16661.
30. Young, A.; Gentzsch, M.; Abban, C. Y.; Jia, Y.; Meneses, P. I.; Bridges, R. J.; Bradbury, N. A. Dynasore Inhibits Removal of Wild-Type and DeltaF508 Cystic Fibrosis Transmembrane Conductance Regulator (CFTR) from the Plasma Membrane. *Biochem. J.* **2009**, *421*, 377–385.
31. Sorkin, A.; Goh, L. K. Endocytosis and Intracellular Trafficking of ErbBs. *Exp. Cell Res.* **2009**, *315*, 683–696.
32. Kumari, S.; Mayor, S. ARF1 is Directly Involved in Dynamin-Independent Endocytosis. *Nat. Cell Biol.* **2008**, *10*, 30–41.
33. Da Costa, S. R.; Yarber, F. A.; Zhang, L.; Sonee, M.; Hamm-Alvarez, S. F. Microtubules Facilitate the Stimulated Secretion of β-Hexosaminidase in Lacrimal Acinar Cells. *J. Cell Sci.* **1998**, *111*, 1267–1276.
34. Mush, A. Microtubule Organization and Function in Epithelial Cells. *Traffic* **2004**, *5*, 1–9.
35. Jerdeva, G. V.; Wu, K.; Yarber, F. A.; Rhodes, C. J.; Kalman, D.; Schechter, J. E.; Hamm-Alvarez, S. F. Actin and Non-Muscle Myosin II Facilitate Apical Exocytosis of Tear Proteins in Rabbit Lacrimal Acinar Epithelial Cells. *J. Cell Sci.* **2005b**, *118*, 4797–4812.
36. Bayer, N.; Schober, D.; Prchla, E.; Murphy, R. F.; Blaas, D.; Fuchs, R. Effect of Bafilomycin A1 and Nocodazole on Endocytic Transport in HeLa Cells: Implications for Viral Uncoating and Infection. *J. Virol.* **1998**, *72*, 9645–9655.
37. Ferreira, D.; Cortez, M.; Atayde, V. D.; Yoshida, N. Actin Cytoskeleton-Dependent and -Independent Host Cell Invasion by *Trypanosoma cruzi* is Mediated by Distinct Parasite Surface Molecules. *Infect. Immun.* **2006**, *74*, 5522–5528.
38. Zieve, G. W. Nocodazole and Cytochalasin D Induce Tetraploidy in Mammalian Cells. *Am. J. Physiol.* **1984**, *246*, C154–C156.
39. Apodaca, G. Endocytic Traffic in Polarized Epithelial Cells: Role of the Actin and Microtubule Cytoskeleton. *Traffic* **2001**, *2*, 149–159.
40. Wood, S. A; Brown, W. J. The Morphology but Not the Function of Endosomes and Lysosomes is Altered by Brefeldin A. *J. Cell Biol.* **1992**, *119*, 273–285.
41. Nel, A. E.; Madler, L.; Velegol, D.; Xia, T.; Hoek, E. M.; Somasundaran, P.; Klaessig, F.; Castranova, V.; Thompson, M. Understanding Biophysicochemical Interactions at the Nano-Bio Interface. *Nat. Mater.* **2009**, *8*, 543–557.
42. Chithrani, B. D.; Chan, W. C. Elucidating the Mechanism of Cellular Uptake and Removal of Protein-Coated Gold Nanoparticles of Different Sizes and Shapes. *Nano Lett.* **2007**, *7*, 1542–1550.
43. Harush, O.; Altschuler, Y.; Benita, S. The Impact of Surface Charge on Nanoparticle Performance. In *Nanoparticles for Pharmaceutical Applications*; Domb, A. J., Tabata, Y., Ravi Kumar, M. N. V., Farber, S., Eds.; American Scientific Publishers: Portland, OR, 200785102.
44. Harush-Frenkel, O.; Altschuler, Y.; Benita, S. Nanoparticle–Cell Interactions: Drug Delivery Implications. *Crit. Rev. Ther. Drug Carrier Syst.* **2008**, *25*, 485–544.
45. Harush-Frenkel, O.; Rozentur, E.; Benita, S.; Altschuler, Y. Surface Charge of Nanoparticles Determines their Endocytic and Transcytotic Pathway in Polarized MDCK Cells. *Biomacromolecules* **2008**, *9*, 435–443.
46. Hillaireau, H.; Couvreur, P. Nanocarriers' Entry into the Cell: Relevance to Drug Delivery. *Cell. Mol. Life Sci.* **2009**, *66*, 2873–2896.
47. Lee, K. D.; Hong, K.; Papahadjopoulos, D. Recognition of Liposomes by Cells: *In Vitro* Binding and Endocytosis Mediated by Specific Lipid Headgroups and Surface Charge Density. *Biochim. Biophys. Acta* **1992**, *1103*, 185–197.
48. Liu, D.; Song, Y. K. Cationic Liposome-Mediated Transfection *In Vivo* (Review). *Gene Ther. Mol. Biol.* **1998**, *2*, 59–68.
49. Kovacs, T.; Karasz, A.; Szollosi, J.; Nagy, P. The Density of GM1-Enriched Lipid Rafts Correlates Inversely with the Efficiency of Transfection Mediated by Cationic Liposomes. *Cytometry A* **2009**, *75*, 650–657.
50. Lai, S. K.; Hida, K.; Man, S. T.; Chen, C.; Machamer, C.; Schroer, T. A.; Hanes, J. Privileged Delivery of Polymer Nanoparticles to the Perinuclear Region of Live Cells *via* a Non-Clathrin, Non-Degradative Pathway. *Biomaterials* **2007**, *28*, 2876–2884.
51. Panyam, J; Labhasetwar, V. Dynamics of Endocytosis and Exocytosis of Poly(D,L-lactide-*co*-glycolide) Nanoparticles in Vascular Smooth Muscle Cells. *Pharm. Res.* **2003**, *20*, 212–220.
52. Panyam, J.; Zhou, W. Z.; Prabha, S.; Sahoo, S. K.; Labhasetwar, V. Rapid Endo-Lysosomal Escape of poly(DL-lactide-*co*-glycolide) Nanoparticles: Implications for Drug and Gene Delivery. *FASEB J.* **2002**, *16*, 1217–1226.
53. Harush-Frenkel, O.; Debotton, N.; Benita, S.; Altschuler, Y. Targeting of Nanoparticles to the Clathrin-Mediated Endocytic Pathway. *Biochem. Biophys. Res. Commun.* **2007**, *353*, 26–32.

54. Yacobi, N. R.; Malmstadt, N.; Fazlollahi, F.; DeMaio, L.; Marchelletta, R.; Hamm-Alvarez, S. F.; Borok, Z.; Kim, K.-J.; Crandall, E. D. Mechanisms of Alveolar Epithelial Translocation of a Defined Population of Nanoparticles. *Am. J. Respir. Cell Mol. Biol.* **2009**, *42*, 604–614.
55. Bareford, L. M.; Swaan, P. W. Endocytic Mechanisms for Targeted Drug Delivery. *Adv. Drug Delivery Rev.* **2007**, *59*, 748–758.
56. Chang, E.; Thekkek, N.; Yu, W. W.; Colvin, V. L.; Drezek, R. Evaluation of Quantum Dot Cytotoxicity Based on Intracellular Uptake. *Small* **2006**, *2*, 1412–1417.
57. Jamieson, T.; Bakhshi, R.; Petrova, D.; Pocock, R.; Imani, M.; Seifalian, A. M. Biological Applications of Quantum Dots. *Biomaterials* **2007**, *28*, 4717–4732.
58. Bender, J. L.; Corbin, P. S.; Fraser, C. L.; Metcalf, D. H.; Richardson, F. S.; Thomas, E. L.; Urbas, A. M. Site-Isolated Luminescent Europium Complexes with Polyester Macroligands: Metal-Centered Heteroarm Stars and Nanoscale Assemblies with Labile Block Junctions. *J. Am. Chem. Soc.* **2002**, *124*, 8526–8527.